applied sciences

MDPI

Article

Role of Functional Monomers upon the Properties of Bisphenol A Molecularly Imprinted Silica Films

Ana-Mihaela Gavrila [1], Ionut-Cristian Radu [2], Hermine Stroescu [3], Anamaria Zaharia [1], Elena-Bianca Stoica [1], Ana-Lorena Ciurlica [1], Tanţa-Verona Iordache [1,*] and Andrei Sârbu [1,*]

[1] Advanced Polymer Materials and Polymer Recycling Group, The National Institute for Research & Development in Chemistry and Petrochemistry ICECHIM, Splaiul Independentei no. 202, 060021 Bucharest, Romania; anamihaela.florea@gmail.com (A.-M.G.); anamaria.lungu1984@gmail.com (A.Z.); elena.bianca.georgescu@gmail.com (E.-B.S.); analorena11.ac@gmail.com (A.-L.C.)

[2] Advanced Polymer Materials Group, University Politehnica of Bucharest, 060042 Bucharest, Romania; radu.ionucristian@gmail.com

[3] Institute of Physical-Chemistry "Ilie Murgulescu" of Romanian Academy, Surface Chemistry and Catalysis Laboratory, 060021 Bucharest, Romania; hermine25@yahoo.com

* Correspondence: tanta-verona.iordache@icechim.ro (T.-V.I.); andr.sarbu@gmail.com (A.S.); Tel.: +4-0755-159-896 (T.-V.I.); +4-0724-237-351 (A.S.)

Abstract: In this study, two types of bisphenol A molecularly imprinted films (BPA-MIP) were successfully prepared via sol-gel derived methods using two different organosilane functional monomers N-(2-aminoethyl)-3-aminopropyltrimethoxysilane (DAMO-T) or (3-mercaptopropyl)trimethoxysilane (MPTES). The physical-chemical characterization of films, in terms of morphology, structure, thermal analysis, and optical features, suggested that thinner films with a homogenous porous structure were more likely to retain BPA molecules. The MIP films revealed the rapid and quantitative adsorption of BPA, registering the most specific binding in the first five minutes of contact with the BPA-MIP film. Silica films were effectively regenerated for further usage for at least five times, demonstrating their high stability and reusability. Even if the performance of films for BPA uptake dropped dramatically after the third adsorption/reconditioning cycle, this synthesis method for BPA-MIP films has proven to be a reliable and cheap way to prepare sensitive films with potential application for re-usable optical sensors.

Keywords: sol-gel; molecularly imprinted films; bisphenol A; organosilane monomer

Citation: Gavrila, A.-M.; Radu, I.-C.; Stroescu, H.; Zaharia, A.; Stoica, E.-B.; Ciurlica, A.-L.; Iordache, T.-V.; Sârbu, A. Role of Functional Monomers upon the Properties of Bisphenol A Molecularly Imprinted Silica Films. *Appl. Sci.* **2021**, *11*, 2956. https://doi.org/10.3390/app11072956

Academic Editor: Raed Abu-Reziq

Received: 26 February 2021
Accepted: 24 March 2021
Published: 25 March 2021

1. Introduction

Bisphenol A (BPA) [2,2-bis (4-hydroxyphenyl)propane], an endocrine disruptor chemical (EDC), is known as the most widely used and toxic additive in the production of plastic together with polycarbonates, epoxy and polyester resins, and others (flame retardants, polyacrylate, polysulfone resins, polyetherimide). Many studies revealed that BPA leaches out from plastic products used for food packaging such as: plastic (baby) bottles, industrial supplies, dental sealant, medical devices, or sport equipment [1–4]. Despite the ongoing COVID-19 pandemic that has affected the sales of paints and coatings in 2020, the global volume consumption of BPA is growing dynamically and is estimated to reach more than ten million metric tons by 2022 [5]. In 2019, the European Commission decided to form a research cluster namely EURION to find novel testing and screening methods to identify EDC [6]. BPA is easily released into the atmosphere and the natural environment through direct discharge, landfill leachate, is and frequently found in food and water sources [7,8]. Long-term exposure to BPA alters endocrine function, causing many diseases as diabetes, obesity, cardiovascular diseases, chronic respiratory, thyroid and immune systems diseases, and even cancer [9–11]. Exposure to BPA occurs mostly via the oral route (approximately 90%) meaning dietary contamination and non-dietary sources such as sea water and cosmetics [12]. So far, several analytical methods have been established and

extensively used to measure BPA, from which gas chromatography–mass spectrometry (GC-MS), immunoassay detection, liquid chromatography–mass spectrometry (LC-MS), and spectrophotometric and optical sensors are frequently used [13]. Yet, most of these methods are expensive, with time-consuming manipulation steps, complicated instrumentation, highly skilled operators, and a large amount of chemicals. Notwithstanding the many available techniques, there is an urgent need to establish a simple, rapid, and low-cost method for monitoring BPA.

Ever since molecular recognition systems with artificial receptors have emerged, the attention of the research community for designing effective separation systems and chemical/sensors has increased significantly. Such molecular recognition systems, named molecularly imprinted polymers (MIPs) are prepared using the molecular imprinting (MI) technique. This is a versatile and inexpensive method to synthesize artificial polymers that mimic the behavior of natural receptors binding sites. The procedure usually involves the polymerization and crosslinking of functional monomers in the presence of a template molecule (that interacts with the polymer network via hydrogen, covalent, or ionic bonding interactions. After the removal of the template molecule, specific binding cavities toward the target molecules are left in the resulting polymers. Thus, the complementary molecular information of the template is transposed into the polymer, endowing the final material with specificity for this analyte but also with selectivity vs. other structural-resemblant analytes. Furthermore, the resulted MIPs are robust, exhibiting reusability, long-term stability and low production cost [14,15]. Using this MI technique and the various polymerization procedures, MIPs in different shapes and sizes were developed, e.g., pearls [16], particles [17,18], membranes [19–21], thin films [22,23], nanospheres/nanofibers [24,25], or electrochemical sensing receptors [13,17,26]. Nevertheless, depending on the polymerization procedure (for instance bulk polymerization [27]), MIPs can still present some inherent drawbacks, such as heterogeneous distribution of binding sites, low binding capacity, and poor site accessibility, which is why a great deal of attention should be focused on finding the proper procedure for delivering performant MIPs adequate for the targeted application. In this context, the preparation of MIPs for sensing applications was performed, in recent years, by combining MI with sol–gel techniques as an alternative approach to overcome these shortcomings [28,29]. The method is simple and implies deposition/casting of thin films on various surfaces (for example nanowires, nanotubes, glass, ceramic and plastic substrates).

Literature studies are minimal when it comes to BPA imprinting for obtaining MIP films via sol-gel methods. One of these studies include that of Huang et al. [30], who described the electrochemical deposition of imprinted sol-gel films with specific binding sites for BPA on a gold electrode. This work implied the use of expensive nanomaterials and the minimal characterization of the sol-gel film hampers the assessment of efficiency. A recent study of Yang and Park [31] used the surface-initiated atom transfer radical polymerization (SI-ATRP) for the synthesis of BPA-imprinted poly(4-vinyl pyridine-co-ethylene glycol dimethacrylate) films on a specific surface of silica inverse opal-formed quartz crystals (QCs). It is also worth mentioning the paper of Ardekani et al., who prepared molecularly imprinted nanofibers based on 3-aminopropyltriethoxysilane (APTES) as functional monomer and nylon 6 as the matrix, using the sol-gel and the electrospinning techniques, which can absorb BPA in water samples [32]. Another valuable study of Kalogiouri and co-workers [33] reported the use of APTES and phenyl triethoxysilane to prepare imprinted sol-gel sorbents for the BPA removal from moat waters and tap water. Although the MIP sorbent can be used up to ten times, the extraction protocol involves numerous steps and materials.

With regard to the recent literature, the present study provides a simpler and more reproducible procedure to prepare BPA-MIPs, with the use of MI and sol-gel derived techniques. The methodology is original and consisted of casting the BPA-MIP layer on top of previously degreased glass support. According to the present literature, this combined procedure of BPA imprinting has never been used to prepare MIP films.

Thereby, the aim of this work was to prepare and characterize two types of BPA-MIP films, based on two different organosilane monomers, meaning N-(2-aminoethyl)-3-aminopropyltrimethoxysilane (DAMO-T) and (3-mercaptopropyl)trimethoxysilane (MPTES). The films BPA-MIP_{DAMOT} and BPA-MIP_{MPTES} were obtained by spraying the sol-gel precursor solutions directly on previously degreased glass slides. The proposed sol-gel approach for BPA-MIP preparation seemed to be suitable due to the low temperature processing conditions (for polycondensation at 25 °C and for the maturation of films at 60 °C). The prepared BPA-MIP films were well characterized by Fourier-Transform Infrared spectroscopy (FTIR), Scanning Electron Microscopy (SEM), and Atomic Force Microscopy (AFM), as well as thermogravimetric analysis (TGA). The optical behavior of films was investigated by ellipsometry, to establish the imprinting effect over the final properties of the obtained BPA-MIPs. The BPA-MIP films were further tested in terms of rebinding measurements in liquid state via spectrophotometric techniques, to assess their potential as sensing elements for optic sensors. The reusability and stability of the sol-gel films were also discussed.

2. Experimental Section

2.1. Materials

The functional organosilane monomers N-(2-aminoethyl)-3-aminopropyltrimethoxysilane (DAMO-T, 98%), (3-Mercaptopropyl) trimethoxysilane (MPTES, 98 %), tetraethoxysilane (TEOS, 98 %), and the template Bisphenol A (BPA, 99%) were all purchased from Sigma-Aldrich Co. (St. Louis, MO, USA). Ammonium hydroxide (NH_4OH, 25 %) as catalyst and other solvents like acetic acid (AcA), obtained from Chimopar (Bucharest, Romania) were used as received. Ethanol (EtOH, 99.6%) was supplied by Fisher Scientific (Schwerte, Germany). The organic solvents used were analytical grade. Distilled water obtained from our laboratory purification system was used to prepare all aqueous solutions. The glass supports were obtained from Sigma-Aldrich Co. (St. Louis, MO, USA).

2.2. Instruments and Characterization

All measurements were performed at room temperature (RT considered 25 °C). The prepared BPA-MIP and NIP films were analyzed morpho-structurally and thermally using various equipment and techniques. Fourier Transform Infrared Spectroscopy (FTIR) of films was performed on Bruker Tensor 37 (ATR) in 400–4000 cm^{-1} domenium, a resolution of 4 cm^{-1} and 16 scans. Thermogravimetric analysis (TGA) was carried out under nitrogen atmosphere at a 10 °C/min heating rate with TA Q2000 IR Instrument with auto-sampler. The thermal stability of sol-gel films was investigated in order to underline the effect of imprinting upon the organosilica materials, as complementary results to FTIR measurements. Estimation of films thickness was made by ellipsometry with UV-VIS-NIR Ellipsometer VASE® model (J.A. Woollam Co, Inc., Lincoln, NE, USA), in the 300–1000 nm wavelength range at 70 °AOI with a 2 nm wavelength step and 20 scans/measurement (microspot). It is relevant to note that a translucent scotch tape was fixed on the glass slides back in order to prevent the effect of 'backside reflection'. The surface morphology of the films deposited on glass slides was investigated with an Environmental Scanning Electron Microscope (ESEM) FEI Quanta 200 from Philips, equipped with gaseous secondary electron detector (GSED). Topography was performed by Atomic Force Microscopy using XE 100 instrument from Park Systems, in non-contact tapping mode at resonance frequency of Z-scanner: 5 kHz. All AFM measurements were recorded using silicon tips with a scan range of XY-scanner of (max) 50 μm, and a working distance of Z-scanner: 12 μm. The AFM images were elaborated with the XEI program (v 1.8.0—Park Systems) for exhibiting roughness evaluation. The UV-2501-PC spectrometer (Shimadzu Co., Tokyo, Japan) was used to perform the BPA batch re-binding experiments and the washing procedures for BPA removal in the 200–1000 nm wavelength range, with a 10 mm quartz cuvette.

2.3. Synthesis of Bisphenol A-Molecularly Imprinted Polymer (BPA-MIP) Films

Two types of BPA-imprinted organosilica films (i.e., BPA-MIP_{MPTES} and BPA-MIP_{DAMOT}) were successfully prepared by directly spraying the precursor solutions on glass supports, according to a similar one-step procedure described by our group, with slight modifications [34]. In a typical batch for BPA-MIP preparation, two solutions were prepared separately at room temperature (RT considered 25 °C), the catalyst and the precursor solution. The catalyst consisted of an aqueous solution of 25% ammonia hydroxide (0.565 mL NH_4OH/0.225 mL H_2O). The precursor solution was prepared by dissolving the functional monomer DAMO-T or MPTES and the template BPA in 1 mL of ethanol under stirring (molar ratio monomer: BPA = 10:1). After stirring for 30 min at 200 rpm, in the precursor solution containing DAMO-T a structural monomer (0.13 mL TEOS) was also added to ensure the adhesion to the glass support. The precursor monomer solution was magnetically stirred for 1 h after which it was gradually added in the catalytic medium and mechanically stirred at 200 rpm, for 2 h (sol-gel time, tsg), when the partial hydrolysis reaction occurs, generating sols. The resulted solution was applied by directly spraying it onto cleaned glass supports to form crosslinked networks by alcohol/aldol polycondensation of sols. The obtained films were maturated for 48 h at 25 °C (until complete polycondensation), followed by curing for 48 h at 60 °C in an oven.

The cured films were then washed two times according to the following procedure: step 1—washing with ethanol, for 8 h at room temperature, for removing unreacted monomers and step 2—extraction of BPA molecules with ethanol-acetic acid (9:1, v/v) for 4 h assisted by ultrasound (at 35 kHz frequency). As shown in Figure S1, a rigorous control of the supernatant solutions was performed by UV-Visible spectroscopy in order to assess the efficiency of the washing/extraction procedures. It can be observed in the second washing/extraction cycle that BPA was successfully extracted from the imprinted films (as confirmed by the absence of specific absorption peaks of BPA). Afterward, all films were dried at 60 °C overnight until constant weight and stored in dried conditions until use. By contrast, non-imprinted control films (noted by analogy NIP) were synthesized, conditioned, and washed respecting the same procedures as for the MIPs; the only difference was the absence of BPA from the synthesis.

2.4. Batch Binding Measurements and Regeneration of BPA Films

Binding experiments were performed to investigate the specificity of MIP films by measuring the adsorbed amount of BPA onto MIPs and NIPs. The binding tests referred to contacting the MIP and NIP films with 35 mL BPA solution of a known concentration (experiments conducted in batch conditions in duplicate) and measuring the initial and the final concentration of BPA. Due to BPA poor solubility in water, organic solvent-based assays were employed. The UV–visible absorption spectrum of bisphenol A in ethanol is given in Figure S2. The specific wavelengths of bisphenol A were registered at 229 nm and 278 nm. Since the value at 229 nm is susceptible to the influence of the solvent, the quantification of BPA was performed against the value at 278 nm as characteristic wavelength for BPA adsorption [35]. Thus, the calibration of BPA at λ = 278 nm was obtained in ethanol using a series of standard solutions containing BPA in the 0.2–0.008 g/L concentration range. The concentration of BPA was found to have a good linear relationship with r^2 = 0.997 (according to Figure S3). Herein, the concentration limits chosen for the study, meaning 0.008 and 0.2 g/L, represented the lowest and the highest quantity of BPA that can be detected by UV.

The kinetic of BPA rebinding was studied in the first 120 min of contact with 0.2 g/L BPA solution in ethanol. Afterward, using various concentrations of BPA (i.e., 0.2, 0.15, 0.1, and 0.08 g BPA/L in ethanol), the adsorbed amount of BPA was measured after a period of only 5 min, considered proper for specificity.

The reusability of the BPA-MIPs and NIPs deposited on glass slides was also investigated by using the same batch of films through the adsorption-desorption studies in five consecutive cycles.

The re-binding capacities, Q (mg BPA g^{-1} polymer film), of BPA-MIP and NIP films were calculated using Equation (1); where $C_{N,i}$ (g/L) and $C_{N,f}$ (g/L) are the initial and final concentration of BPA in the feed solution, m_p (mg) the films weight ($m_p = 40 \pm 1$ mg) and V_S (L) is the volume of the feed solution (i.e., 35 mL).

$$Q = \frac{(C_{N,i} - C_{N,f}) \cdot V_s}{m_p} \quad (1)$$

Imprinting factors, F, expressed by Equation (2), quantified the specificity with which BPA-MIP films re-bind BPA, compared to their corresponding NIPs, where Q_{MIP} and Q_{NIP} are the re-binding capacities of BPA-MIP and NIP, respectively.

$$F = \frac{Q_{MIP}}{Q_{NIP}} \quad (2)$$

3. Results and Discussion

3.1. Preparation of the BPA-MIP Films

This work was aimed at obtaining BPA-MIP films having two different organosilane functional monomers i.e., DAMO-T and MPTES. It is worth to mention that sol-gel hybrid films have attracted attention due to their efficient immobilization on various substrates, their enhanced stability and, in this case, easy access to the recognition cavities thus created. In this respect, the MPTES organosilane monomer was chosen for its adhesive properties and the ability to interact with the template, whereas DAMO-T monomer was expected to create stronger interactions with the template due to its diamino functionalities. For the later formulation, the adhesive properties to the substrate were compensated by addition of TEOS. Furthermore, the preparation method of films via sol-gel was very simple, quick, and did not require expensive chemicals or instrumentation.

The synthesis recipes for the precursor solutions used to obtain BPA-MIP and NIP films are given in Table 1. Previously reported results showed that aromatic templates are difficult to extract from MIP films with over 4–5 μm thickness and thinner films under 100 nm detach from the glass slide after multiple washing procedures [21]. Therefore, the monomer(s)/solvent/catalyst ratios were similar to the ones reported previously.

Table 1. The synthesis recipes for control NIP and BPA-MIP films.

Notation	DAMO-T (mmoles)	MPTES (mmoles)	TEOS (mmoles)	BPA (mmoles)
$BPA\text{-}MIP_{MPTES}$	0	0.364	0	0.0364
NIP_{MPTES}	0	0.364	0	0
$BPA\text{-}MIP_{DAMOT}$	0.364	0	0.0058	0.0364
NIP_{DAMOT}	0.364	0	0.0058	0

The schematic representation for BPA imprinting in sol-gel films and deposition on glass substrates is given in Figure 1. An alkaline solution (1 N NaOH) was used to clean the surface of the glass substrates before film casting. The cleaning per glass slide was carried out in triplicate by immersing it in 10 mL of alkaline solution for 30 min. Finally, it was dried in a vacuum oven at 60 °C for 2 h. Herein, monolayers of polymeric films were prepared by spraying the obtained precursor solutions directly on cleaned glass substrates. In the first step, following the MI principle, a polymerizable complex between the organosilane precursors DAMO-T or MPTES and BPA molecules is formed in ethanol and, further on, a partial hydrolysis of this assembly takes place in basic medium (NH_4OH, H_2O) [22]. The second step consists of sols formation [34]. Non-hydrolyzed and partially hydrolyzed DAMO-T/MPTES-BPA molecules undergo a polycondensation reaction to form cross-linked and homogeneous tridimensional networks in the third step [14,36]. After

a suitable maturation/curing protocol [28], the hybrid MIP films were washed several times and BPA was properly extracted with the formation of specific imprints.

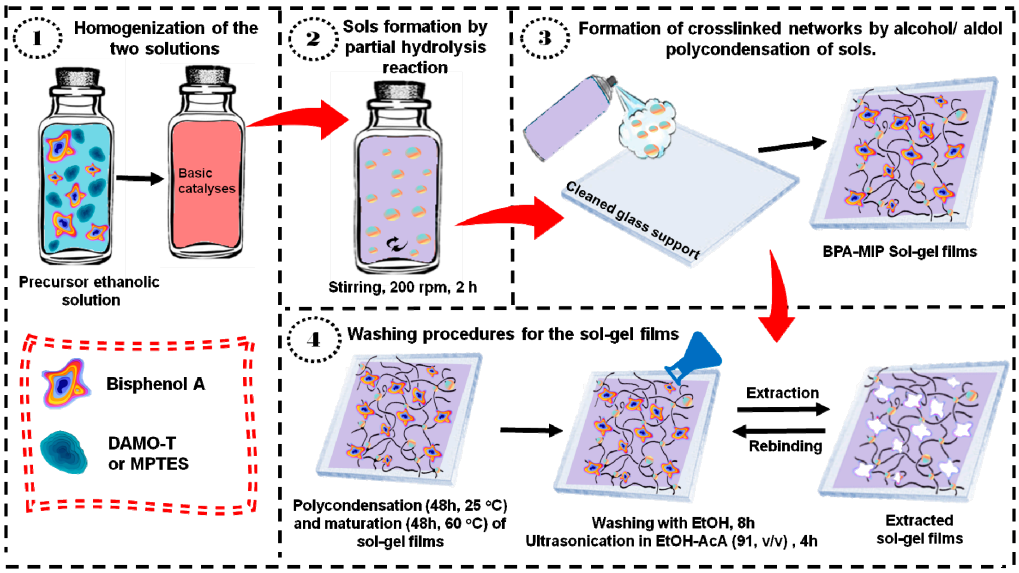

Figure 1. Steps undertaken for the preparation of the BPA-MIPs films.

3.2. Structure of BPA-MIP and NIP Films

FTIR spectroscopy was used to characterize the films and specifically to prove the presence of BPA molecules upon the organosilica matrix. In Figure 2a,b, FTIR spectra of imprinted sol-gel films BPA-MIP$_{MPTES}$ and BPA-MIP$_{DAMOT}$ and non-imprinted homologues NIP$_{MPTES}$ and NIP$_{DAMOT}$, respectively, were compared with the spectrum of BPA template molecule. FTIR analysis of BPA-MIP and NIP films presented some similarities and showed the main characteristic polymeric bands.

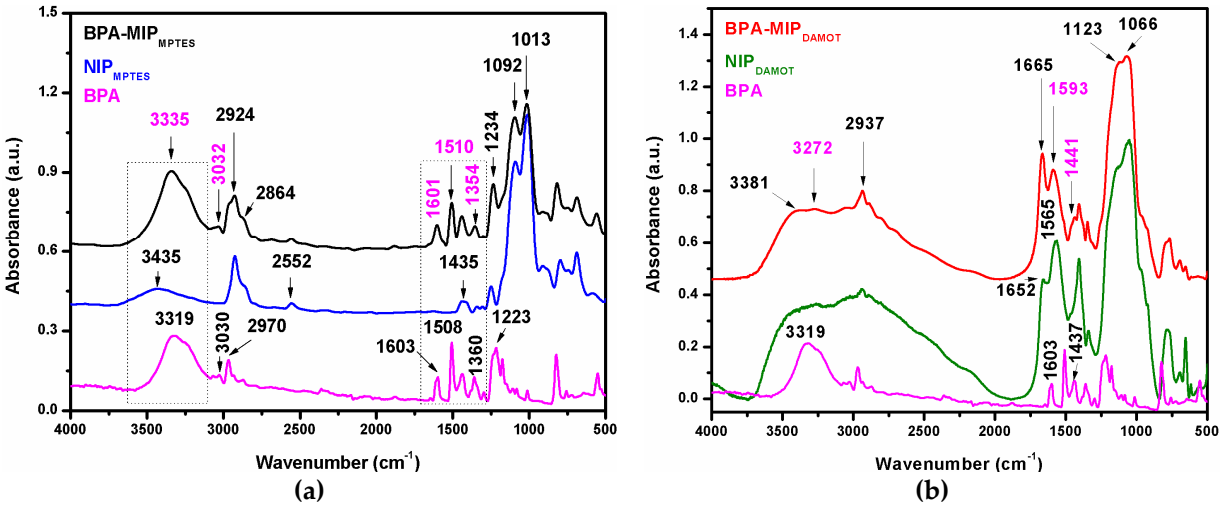

Figure 2. FTIR spectra (KBr pellets) of (**a**) BPA-MIP$_{MPTES}$ and corresponding NIP$_{MPTES}$ and (**b**) BPA-MIP$_{-DAMOT}$ and its control NIP$_{DAMOT}$ sol-gel films, compared to the spectrum of BPA.

The stretching vibrations characteristic to the organic functionalities of the two monomers, ν_{-CH2} and ν_{-CH-}, recorded in the 2950–2920 cm^{-1} and 650–680 cm^{-1} region were observed in the spectra of all films. Distinctive bands of the organosilica backbone network (i.e., Si-O-Si, Si-OH and Si-O stretching vibrations) were identified in all the spectra of films in the 1250–850 cm^{-1} spectral range (bands overlapping in the spectra of

BPA-MIPs and NIPs). For MPTES-based films (Figure 2a), the band at 2552 cm^{-1} revealed the presence of mercapto group (-SH) in the organosilica matrix. In addition to mercapto band, other characteristic bands in the BPA-MIP_{MPTES} spectrum were distinguished as follos: the bands of the methoxy groups, asymmetric ν_{asym} (Si–OCH_3) and symmetric ν_{sym} (Si-OCH_3) stretching vibrations at 2924 and 2864 cm^{-1}. In Figure 2b, spectra of films with DAMO-T, some of the characteristic bands of N-H bonds form DAMO-T were spotted at 3381 cm^{-1} (ν_{N-H}) and the bending vibrations at 1652 cm^{-1} (δ_{N-H}). The results indicate that the organosilica functional monomers were quantitatively incorporated into the hybrid crosslinked networks by alcohol/aldol polycondensation of DAMO-T or MPTES.

In the spectrum of BPA (Figure 2a,b), we can distinguish the characteristic band of the aromatic ring $\nu_{C=C}$ (Ar-C=C) recorded at 1603 cm^{-1} and bands recorded at 1508, 1437, and 1360 cm^{-1} assigned to the C-H bending. The stretching vibrations from 3319 cm^{-1} (very intense band) and 2970/3030 cm^{-1} were assigned to the ν_{OH} (Ar-OH) and ν_{-CH3-} (C-CH_3) bonds, respectively. The band recorded at 1223 cm^{-1} is due to C-O stretching. Figure 2a also revealed the characteristic bands of BPA in the spectrum of BPA-MIP_{MPTES} film, meaning the aromatic rings vibration at 1601 cm^{-1}, the bands for C-H bending at 1510 cm^{-1}, 1437, and 1354 cm^{-1} and the stretching of C-O bonds given by the spiked intensity of the band at 1234 cm^{-1}, indicating that BPA molecules were successfully imprinted in the matrix [37,38]. For BPA-MIP_{DAMOT}, Figure 2b, these bands overlap with those of DAMO-T. Yet, a hint to BPA imprinting was given by the significant shifting of bands from 1652 and 1565 cm^{-1} (in the spectrum of NIP) to 1665 and 1593 cm^{-1} (in the spectrum of BPA-MIP_{DAMOT}) and the presence of a band assigned to C-H bending at 1441 cm^{-1}.

The bands at 3335 cm^{-1} (sharp band) and 3032 cm^{-1} in BPA-MIP_{MPTES} and 3272 cm^{-1} (wide band) in BPA-MIP_{DAMOT} spectra were attributed to the stretching and bending mode of O-H groups from BPA implied in the monomer-template interactions through hydrogen bonding. When comparing the spectra of the two imprinted films, it is important to point out that a more visible imprinting effect was highlighted for BPA-MIP_{MPTES} (as compared to BPA-MIP_{DAMOT}).

3.3. Morphology of BPA-MIP and NIP Films

The surface morphology evaluation of prepared sol-gel films was firstly explored by scanning electron microscopy (SEM, Figure 3) and, afterwards, with atomic force microscopy (AFM, Figure 4). The SEM images of BPA-MIP_{MPTES} and BPA-MIP_{DAMOT} and their corresponding NIP_{MPTES} and NIP_{DAMOT}, respectively, are presented in Figure 3, where significant changes of surface morphology can be noticed. The micrographs of BPA-MIPs and NIPs films clearly indicated morphological differences even though the main network is chemically resemblant (Si-O-Si).

Comparing the morphology of the NIPs with that of BPA-MIPs, the difference was striking. NIP films presented smoother surfaces with little visible asperities or pores, ascribed to the absence of imprinted sites. An overview at lower scales revealed an aggregated structure of the NIP_{MPTES} film (Figure 3b) with rather large gaps instead of pores. Interestingly, BPA-MIP_{MPTES} exhibited a dense structure of pores consisting of aggregated sols, in which case it can be due to the presence of monomer-template assemblies that clearly influenced the growth mode of the entire sol-gel network (Figure 3a). This porous structure of BPA-MIP_{MPTES} films is very beneficial for the mass transfer, BPA rebinding, and may lead to shorter periods for equilibrium adsorption [39]. For BPA-MIP_{DAMOT} films, an interesting, elongated structure (like pine branches) was observed in Figure 3c, unveiling again the result of a preferential arrangement and growth of the network in the presence of monomer-template assemblies. Unlike BPA-MIP_{MPTES}, the surface of BPA-MIP_{DAMOT} seemed to be more compact, which may be caused by the addition of TEOS that conferred rigidity to the whole structure.

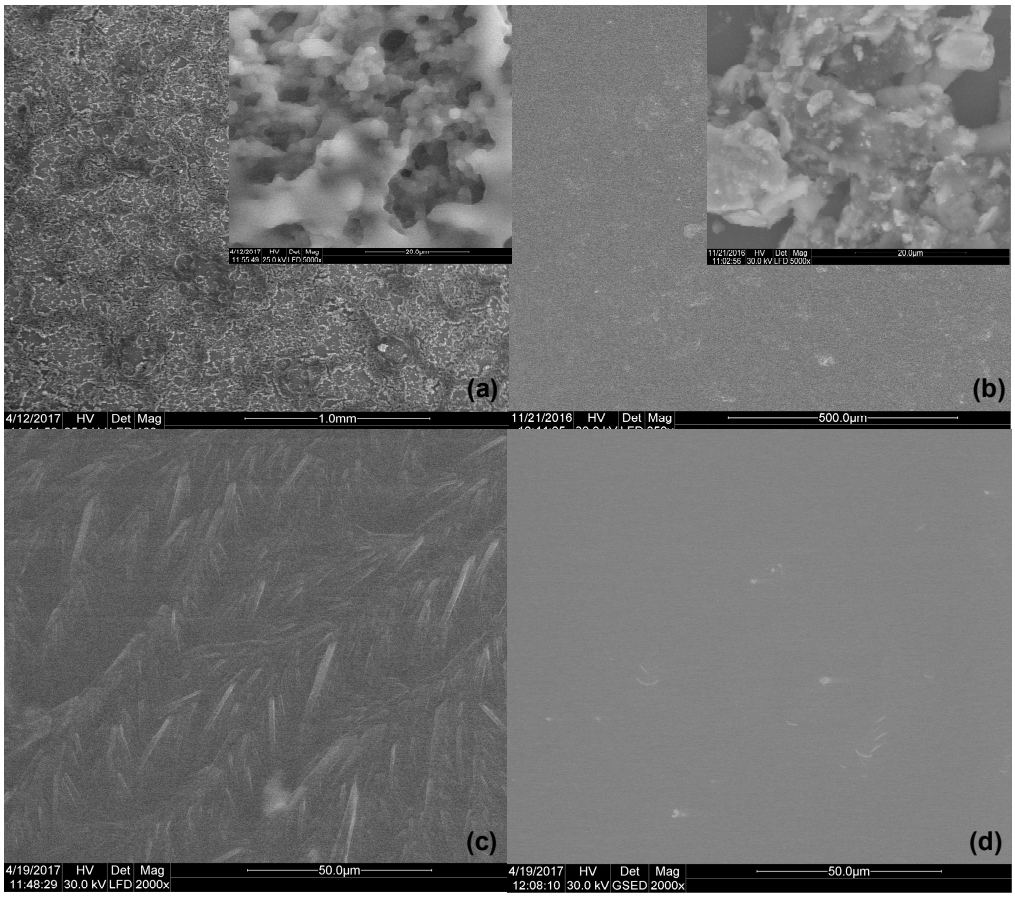

Figure 3. Surface SEM micrographs of both sets of sol-gel films, at different magnitude levels: (**a**) BPA-MIP$_{MPTES}$ and (**b**) NIP$_{MPTES}$ at 1mm/500 µm scale with 20 µm insets (**c**) BPA-MIP$_{DAMOT}$ and (**d**) NIP$_{DAMOT}$ at 50 µm.

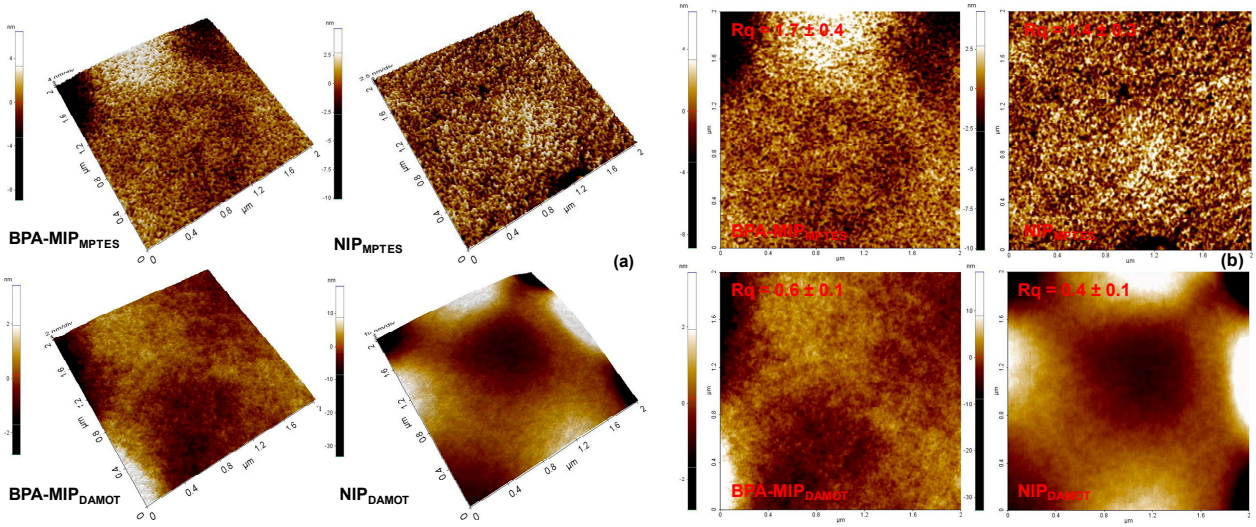

Figure 4. 3D (**a**) and 2D (**b**) topography images by atomic force microscopy (AFM) of the surface of BPA-MIP$_{MPTES}$/BPA-MIP$_{DAMOT}$ films, compared to control NIPs, scan area of 2 × 2 µm; RMSR values included on each AFM image (in red).

The topography and roughness of both BPA-MIP films and their corresponding NIPs were investigated by AFM (Figure 4), as well. The surface roughness of the sol-gel films was evaluated using the root-mean-square roughness (RMSR) function of XEI AFM software.

As shown in Figure 4b, five different topographic images were chosen to calculate the arithmetic average leading to the RMSR results. The AFM images of NIPs and BPA-MIP films emphasized again the changes that occur in surface topography due to the presence of monomer-template assemblies. In agreement with the SEM analysis, the 3D images of the BPA-MIP_{MPTES}/NIP_{MPTES} films (Figure 4a) pair displayed a fully different porous architecture compared to the flatter and smoother surface of the other pair, BPA-MIP_{DAMOT}/NIP_{DAMOT} (Figure 4a). Compared to SEM, the AFM footage revealed a very dense porous structure for the BPA-MIP_{DAMOT} film, as well. Yet, in this case the pore sizes are much smaller than the ones observed on the surface of BPA-MIP_{MPTES}, which may lead to a slow diffusion of BPA during rebinding trials and low binding efficiency [40]. The presence of BPA led to higher surface roughness values for BPA-MIP_{MPTES} and BPA-MIP_{DAMOT} (with a RMSR of 1.7 nm and 0.6 nm, respectively) compared to those of the corresponding NIPs (1.4 nm and 0.4 nm, respectively). The differences of RMSR values can be explained by the presence of template molecules that exert a steric effect during the growth of the sol-gel network. Meaning, the physical volume occupied by the template molecules, which translates later into imprinted cavities, is responsible for the formation of small gaps between the neighboring SiO_2 chains.

Thereby, from the morphological analysis, one conclusion may be drawn with regard to the type of organosilane monomer (or better yet the organic functionalities of the monomer), i.e., the nature of the functionalities influenced the films morphology and the growth pattern of the sol-gel network.

3.4. Thermal Stability of BPA-MIP and NIP Films

Thermogravimetric analysis, performed under nitrogen gas at a 10 °C/min heating rate, indicated similar decomposition trends for the two types of sol-gel films (Figure 5). The thermal degradations of BPA-MIP_{DAMOT} and BPA-MIP_{MPTES} and their non-imprinted NIP_{DAMOT} and NIP_{MPTES} revealed that all films were thermally stable. Three main degradation steps were observed for all the samples. For DAMO-T-based films, a higher mass loss was observed between 50 and 150 °C and it was attributed to the evaporation of intrinsic water, hence confirming the FTIR spectroscopy results where significant amount of water was retained in the structure of DAMO-T-based film.

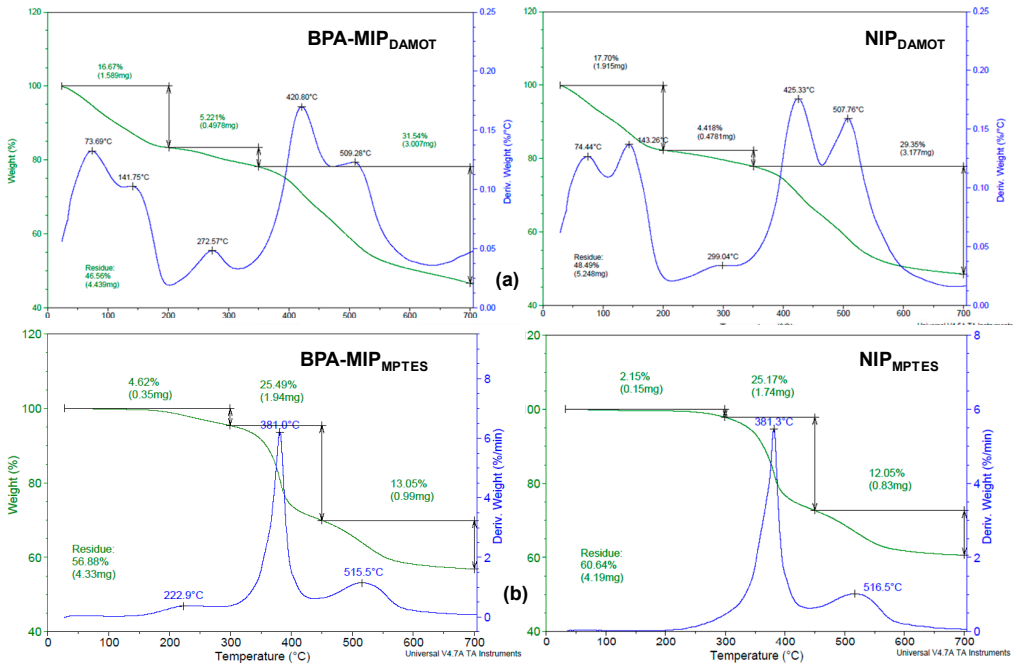

Figure 5. Thermogravimetric curves (TG) and their derivatives (DTG) for (**a**) BPA-MIP_{DAMOT} and NIP_{DAMOT} (**b**) BPA-MIP_{MPTES} and NIP_{MPTES} films.

The first degradation step was recorded in the 200–300 °C temperature range, with maximums registered at 273 °C and 223 °C for BPA-MIP_{DAMOT} and BPA-MIP_{MPTES}, respectively, and attributed to BPA degradation according to the thermogram of BPA provided in Figure S4 (Tmax = 268 °C). The shift to lower or higher maximum decomposition temperatures is not unusual and this observation can help explain two interesting phenomena that may occur during imprinting in soft and rigid sol-gel networks [21,36,41]. For instance, in the case of BPA-MIP_{MPTES} films (Figure 5b), the low stability of BPA indicated that interactions between the template and the functional SH groups of the monomer, potentially weaken the (C-CH_3) bonds from BPA which led to the fragmentation of the molecule. On the other hand, the BPA imprinted in the BPA-MIP_{DAMOT} film (Figure 5a) degraded at higher temperatures due to the inherent rigidity of the sol-gel network, given by the addition of TEOS. It should also be mentioned that a small mass loss was also registered for the NIP based on DAMO-T in this same region and may be linked with the loss of amino fragments from DAMO-T.

The second degradation stage occurred between 300 and 500 °C and was generally attributed with the total degradation/fragmentation of the pendant groups (i.e., methyl/ethyl fragment types, amino-ethyl/methyl, mercaptopropyl). The degradation of the polymer backbone occurred in the last degradation step, between 500–800 °C, [34]. It should be underlined that for both BPA-MIPs the residues were up to 57 wt.% and slightly lower compared to their corresponding NIPs, up to 61 wt.%, confirming a similar behavior between them but also their good thermal stability considering their structural differences.

3.5. Optical Properties of BPA-MIP and NIP Films

The spectroscopic ellipsometry (SE) measurements were performed to highlight the effect of imprinting on the optical properties of films, in terms of refractive index and transmittance. The refractive index of the films was measured in the 200–1000 nm wavelength domenium and the transmittance profiles were evaluated up to 900 nm spectral range, respectively, in different points of the films surface. In this respect, the Cauchy dispersion model was used for modelling the ellipsometric experimental data (Figures S5.1–S5.4, SM) which delivered reliable values for the films thickness and surface roughness.

The thickness and surface roughness for both prepared sets of films, summarized in Table 2, revealed major differences as function of the various employed monomers. For MPTES-based films the thickness varied between 230 and 290 nm, while for the DAMO-T-based films was 10-fold higher. A similar trend was registered for the roughness, as well. The thickness and roughness discrepancy between the two types of films was attributed to the different growth mechanism of the organosilica matrix upon BPA addition and to the presence of TEOS, supporting the results attained in the morphological assessment.

Table 2. Data on films thickness (d_{layer}), roughness and mean square error (MSE) for thickness determined by ellipsometry.

Film	d_{layer} [nm]	Roughness [nm]	MSE
BPA-MIP_{DAMOT}	2897.58	0.62	0.49
NIP_{DAMOT}	3156.57	0.32	0.52
BPA-MIP_{MPTES}	237.36	1.31	0.46
NIP_{MPTES}	290.33	0.97	1.63

Figure 6 shows the refractive index, n, and the transmittance spectra of BPA-MIP_{DAMOT} and BPA-MIP_{MPTES} films against their corresponding NIPs. Pronounced modifications of the optical features (transmittance and refractive index) for both type of films were recorded particularly in the 300–550 nm wavelength region. The variance of refractive index and transmittance presented similar profiles for both MIP films, indicating the presence of BPA in both film structures. The refractive index (Figure 6a) showed great fluctuations for both types of films. For example, the n values registered for the MIP/NIP films with DAMO-T were affected by thickness and, thus, their whole profile is shifted towards higher n values

compared to the MIP/NIP pair with MPTES. However, the same trend is maintained between the imprinted and non-imprinted films suggesting that light travels faster through the non-imprinted material (as lower n values were registered in both cases compared to the ones of MIPs).

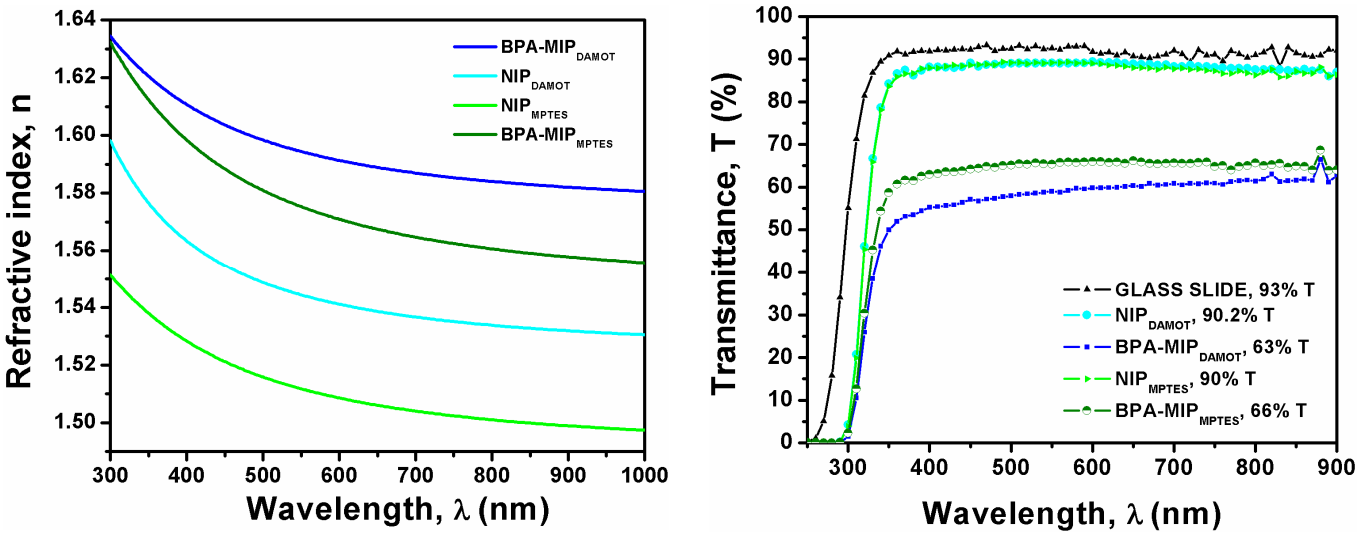

(**a**) (**b**)

Figure 6. Optical properties of BPA-MIP films compared to their corresponding NIP in terms of (**a**) Refractive index, n, variation measured in the 200–1000 nm spectral range and (**b**) Measured transmittance spectra as a function of wavelength, in the 250–900 nm range.

In accordance with the refractive index, the transmittance profiles of the BPA-MIP films registered a drop of about 25% T compared to the NIPs (Figure 6b). This sudden decrease from 90% T to around 66% T was again attributed to the presence of BPA. Yet, the BPA-MIP$_{DAMOT}$ film led to a more obvious decrease of transmittance as the film thickness is 10-fold higher than the one of BPA-MIP$_{MPTES}$.

Both the refractive index and transmittance profiles are consistent with the findings from previous studies [22,34]. These results strengthen the belief that ellipsometric data may better underline the effect of imprinting and the presence of the template when preparing thin and transparent MIP films. Hence, it can be used as a complementary method to characterize the optical features of MIP films and decide upon the potential of such films to be used as sensitive elements for building optical sensors. In addition, the small values of the roughness for the MPTES-based films obtained in this work are considered suitable for optical sensing applications [42].

3.6. Batch Rebinding of BPA on BPA-MIP and NIP Films

The rebinding studies of BPA consisted of adsorption kinetics analysis and isotherm batch adsorption assays, carried out for the two types of BPA-MIP films (i.e., BPA-MIP$_{MPTES}$ and BPA-MIP$_{DAMOT}$) and their corresponding blank NIP$_{MPTES}$ and NIP$_{DAMOT}$ as references. The specificity for BPA uptake was assessed by calculating the adsorption capacities, Q (mg/g) and imprinting factors, F of films (Figure 7a,b). From this point of view, the quantification of bonded BPA was conducted indirectly by determining the un-bonded BPA from the supernatants at 278 nm (characteristic wavelength for BPA absorbance).

Figure 7a shows the adsorption kinetics of the two BPA-MIP films and their corresponding blank NIPs from a 0.20 g/L BPA solution. The adsorption capacity of all films increased rapidly in the first 20 min, especially for the BPA-MIP films. This trend was followed by a plateau after which the binding equilibrium (Qe) was attained, at 60 min. The NIP films presented similar adsorption profiles over time compared to BPA-MIP films

and attained lower values for the adsorption capacity due to the lack of specific binding sites. More importantly, the imprinting factor (F) of BPA-MIP$_{MPTES}$ (Figure 7b) was 3.03 in the first 5 min, indicating not only excellent imprinting of BPA but also the recommended time of contact for attaining the most specific adsorption of BPA.

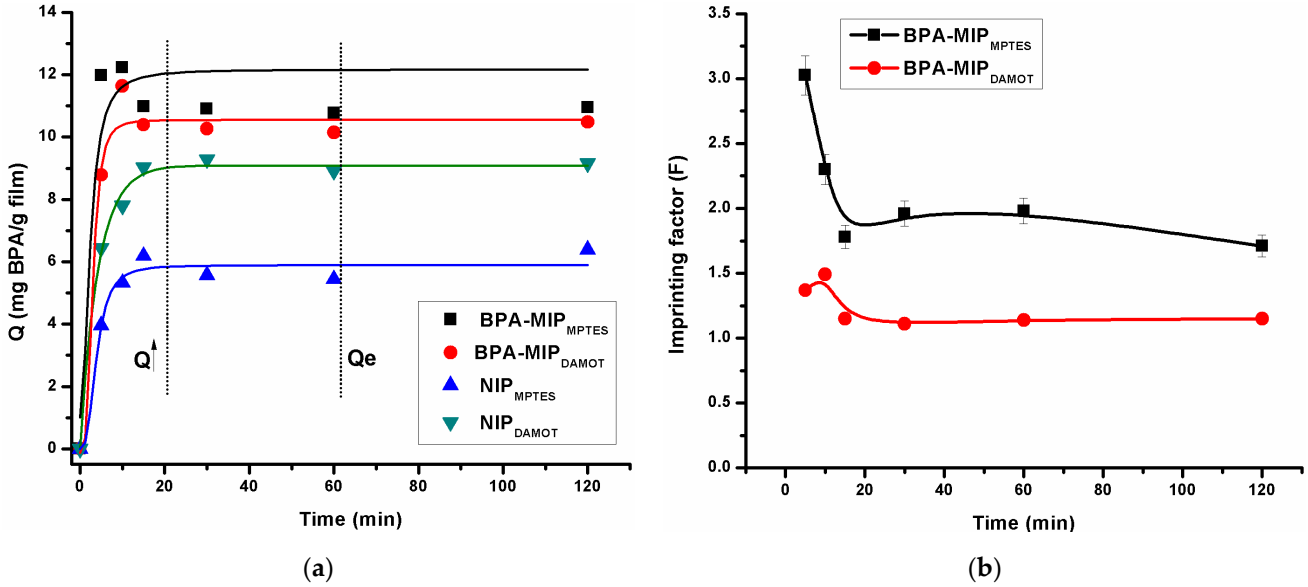

(**a**) (**b**)

Figure 7. (**a**) Adsorption kinetic curves of BPA after contact with BPA-MIP films and their control NIP (variation of Q in mg of BPA per g of BPA-MIP/NIP films) and (**b**) Variation of imprinting factor (F) for both BPA-MIP films over time (5–120 min) from a BPA solution of 0.20 g/L).

As a result, the following isothermal adsorption of BPA in ethanol was determined after only 5 min of contact with the two types of films, in a concentration range varying from 0.08 to 0.2 g/L. As shown in Figure 8, the rebinding amounts of BPA increased gradually with the increasing BPA concentration. The rebinding of BPA, for both BPA-MIP films, exhibited an incremental increase of the adsorption capacity values [28]. As expected, the bonded amount of BPA to the MIP was higher than the one bonded to the NIP. Considering that the concentration of BPA feed solution (Ci) was varied between 0.08–0.20 g/L, the maximum adsorption capacity values were registered at 0.20 g/L, for both the BPA-MIP$_{MPTES}$ and NIP$_{MPTES}$ (Qmax 11.98 and 3.96 mg g^{-1}, respectively). This high difference in BPA binding affinity to the BPA-MIP and NIP clearly indicated the role of the imprinting in the formation of specific binding sites. Moreover, comparing the adsorption capacity values of the two imprinted films, it was observed that BPA-MIP$_{DAMOT}$ registered a maximum adsorption capacity of 8.78 mg/g for the same BPA feed solution (Ci = 0.20 g/L). These results highlighted the impact of the film thickness and the discrete porous structure of BPA-MIP$_{DAMOT}$ film upon the rebinding performance. Chang et al. [2] reported a maximum BPA adsorption of silica MIPs nanospheres of 444.6 µmol g^{-1} and Yang and Park [31] reported a Qmax of 170 mg g^{-1}. Hence, in this case, it seems like thinner films are more efficient for rebinding BPA and the maximum capacities are in good agreement with other reported values.

Considering that the best results were obtained for thinner BPA-MIP$_{MPTES}$ films, it was expected to have better performances for NIP$_{MPTES}$ vs. NIP$_{DAMOT}$ films. Thereby, it seemed like the different growth mechanism of the organosilica matrix upon BPA addition somehow affected the following binding properties of BPA-MIP$_{DAMOT}$ films as compared to the MIP/NIP system with MPTES.

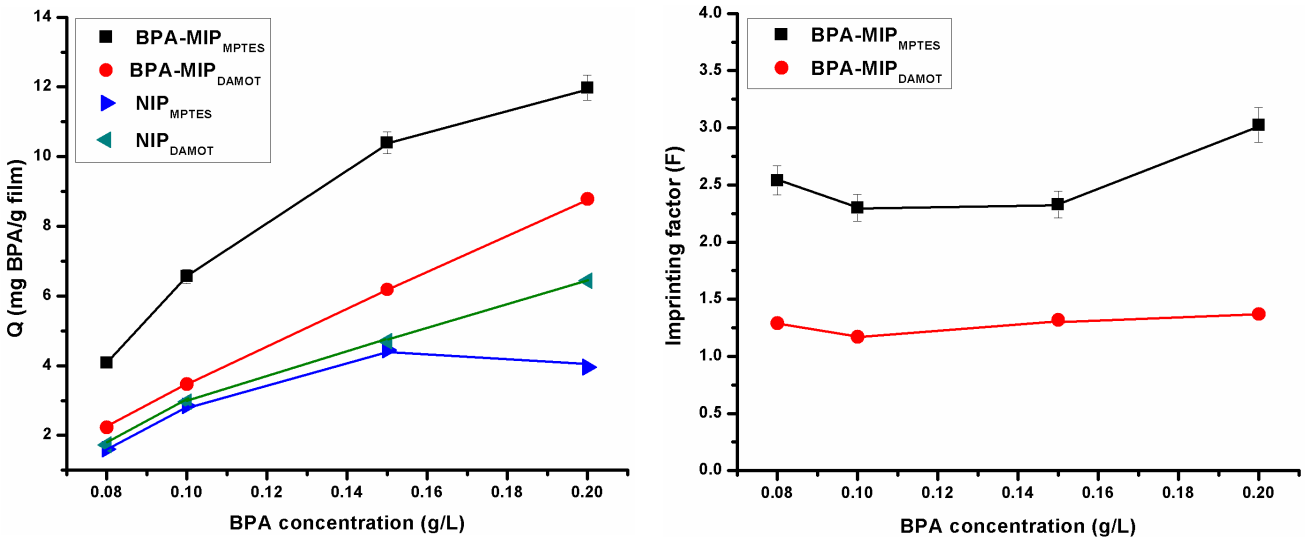

(**a**) (**b**)

Figure 8. Variation of (**a**) binding capacity, Q, in mg of BPA per g of BPA-MIP/NIP films on BPA-MIP films and their control NIP, and (**b**) Imprinting factor (F) obtained by batch experiments after 5 min with various BPA feed solutions, C*i* (0.08–0.2 g/L^{-}).

Nevertheless, both imprinted films, BPA-MIP$_{MPTES}$ and BPA-MIP$_{DAMOT}$, exhibited higher affinity for BPA than the corresponding non-imprinted films leading to the maximum imprinting factors of 3.03 and 1.37, respectively (Figure 8b). Therefore, it can be seen that BPA-MIP$_{MPTES}$ films were more efficient for BPA recognition concluding that the imprinting effect was clearly distinguished by these preliminary batch rebinding tests. The higher values of the imprinting factor and of the binding capacity registered for BPA-MIP$_{MPTES}$, compared to BPA-MIP$_{DAMOT}$ were in agreement with the conclusions drawn from the morpho-structural evaluation of films. According to other reported values for the imprinting factor, such as the one reported for nylon nanofibers (3.4 [32]) and the one reported by Yang and Park (2.15 [31]), the maximum F value of 3.03 found in this study is quite adequate.

3.7. Reusability and Stability of Films

The reusability and stability of the prepared BPA-MIP and NIP films were also evaluated. Reusability and, implicitly, stability are some of the most important features of MIPs due to the fact that are decisive factors for establishing the whole cost-effectiveness of the process. Thereby, in order to evaluate the performance at repeated use, the films were subjected to 5 reutilization cycles. As shown in Figure 9, all the films can be effectively regenerated for further usage with only around 35% loss of the initial rebinding capacity after three cycles, demonstrating high stability and reusability in BPA recognition. After the 4th cycle the binding capacity drops dramatically, up to 65% in the final cycle. Therefore, the BPA-MIP films proved to maintain their structure after several reuse. Yet, it is recommended to use the films only for 3 cycles as the specificity is also altered after the 4th and 5th cycles; the binding capacities of the NIP presented a much lower binding capacity loss. The relative standard deviation (RSD) value of 2.1% ascribed to the good repeatability of the films. It is relevant to mention that all the films were able to withstand the conditions for reconditioning and rebinding for at least five cycles without detaching from the glass support. In terms of long-term stability, the films were kept in dry conditions for several months at room temperature when not in use.

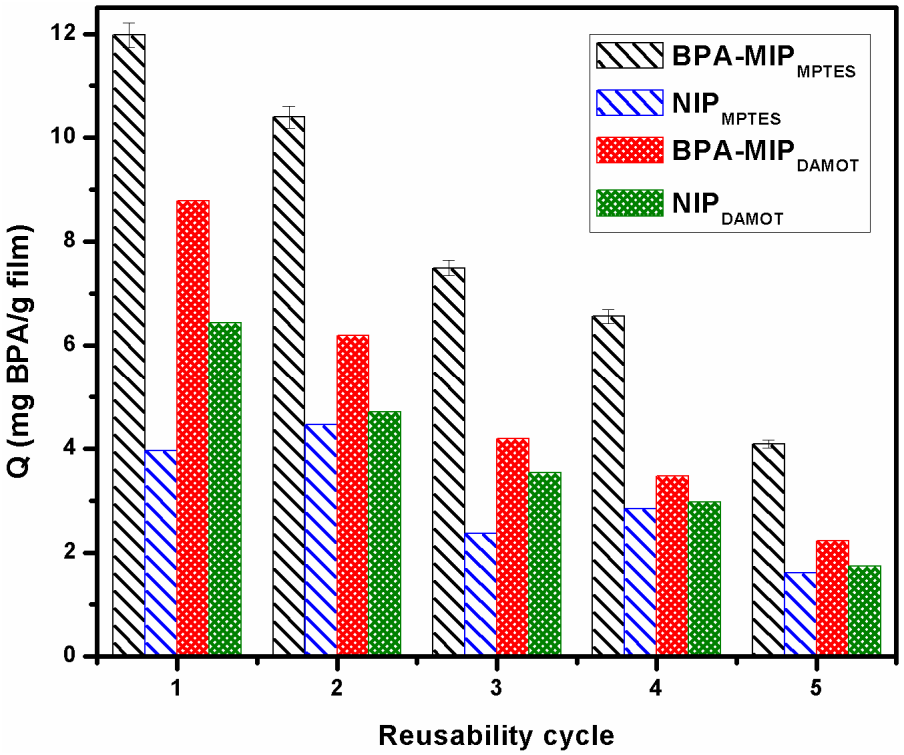

Figure 9. Reusability experiments of BPA-MIP and NIP films.

4. Conclusions

The study provides significant information regarding the role of functional monomers in the molecular imprinting process of BPA in silica networks. The two sets of BPA molecularly imprinted films (i.e., BPA-MIP$_{DAMOT}$ and BPA-MIP$_{MPTES}$) were successfully prepared via sol-gel derived methods using N-(2-aminoethyl)-3-aminopropyltrimethoxysilane (DAMO-T) and (3-mercaptopropyl)trimethoxysilane (MPTES) as functional organosilane monomers.

Morpho-structural, thermal, and optical studies were undertaken to assess the influence of the monomers' functionalities upon the overall features of films but also to highlight the meaningful changes brought by the addition of BPA. Ellipsometry results suggested that there is much potential for application of such BPA-MIP films in optical sensing applications. An evaluation of specificity for BPA was conducted and the relevant results on adsorption capacities and imprinting factors for both types of films- were in agreement with their morpho-structural properties.

The overall results have shown that thinner films with better-defined porous morphology, meaning BPA-MIP$_{MPTES}$ were more likely to retain BPA molecules. In this case, the most specific binding of BPA was registered in the first five minutes after contact (F = 3.03). BPA-MIP films were effectively regenerated for further usage 5 times and the adsorption capacity of films decreased only by 35% after three cycles, demonstrating high stability and reusability.

In order to ascertain the real application potential of the prepared sol-gel imprinted films for BPA detection, the next challenges will assume an investigation of the selective adsorption of BPA-MIP films using compounds with similar structure and application of the methodology for real samples contaminated with BPA. Considering that the BPA-MIPs films enable stability and reusability, the real-time response can be estimated in terms of quantification limit (LOQ) in the range of ng–µg in aqueous samples. Although further investigations are required, this work is a step forward to develop simple and cost-effective molecularly imprinted silica films for optical sensors.

Supplementary Materials: The following are available online at https://www.mdpi.com/2076-3417/11/7/2956/s1, Figure S1: The UV-visible absorption spectra after two steps of washing (1) 1st washing protocol with ethanol and (2) 2nd washing with ethanol-acetic acid (9:1, *v*/*v*) for imprinted BPA-MIP$_{MPTES}$ and BPA-MIP$_{DAMOT}$ and their non-imprinted NIP$_{MPTES}$ and NIP$_{DAMOT}$; Figure S2. UV–visible absorption spectra of 1.5 µg/mL bisphenol A in ethanol; Figure S3. The calibration curve of BPA in ethanol solution; Figure S4. Thermogravimetric curve (TG) and its derivative (DTG) for BPA template; Figure S5. Fitting of the experimental ellipsometric data.

Author Contributions: Conceptualization of the paper by A.-M.G. and T.-V.I.; Methodology by A.-M.G., E.-B.S. and A.-L.C.; Formal analysis by A.-M.G., I.-C.R. and H.S.; Investigation by A.Z.; Writing of Original Draft was done by A.-M.G. and T.-V.I.; Writing—review and editing by T.-V.I.; Supervision by A.S.; Project administration by A.S., T.-V.I.; All authors have read and agreed to the published version of the manuscript.

Funding: This research was funded by Romanian Funding Agency UEFISCDI, through the supporting projects NUCLEU PN.19.23.02.01. and by the 255PED/2020.

Institutional Review Board Statement: Not applicable.

Informed Consent Statement: Not applicable.

Data Availability Statement: The data presented in this study are available in the article.

Conflicts of Interest: The authors declare no conflict of interest.

References

1. Ensafi, A.A.; Amini, M.; Rezaei, B. Molecularly imprinted electrochemical aptasensor for the attomolar detection of bisphenol A. *Microchim. Acta* **2018**, *185*, 265. [CrossRef] [PubMed]
2. Chang, T.; Yan, X.; Liu, S.; Liu, Y. Magnetic Dummy Template Silica Sol–Gel Molecularly Imprinted Polymer Nanospheres as Magnetic Solid-Phase Extraction Material for the Selective and Sensitive Determination of Bisphenol A in Plastic Bottled Beverages. *Food Anal. Methods* **2017**. [CrossRef]
3. Dermer, O.C. *Encyclopedia of Chemical Processing and Design*; McKelta, J.J., Weismantel, G.E., Dekker, M., Eds.; Publisher: New York, NY, USA, 1999; p. 406.
4. Rubin, B.S. Bisphenol A: An endocrine disruptor with widespread exposure and multiple effects. *J. Steroid Biochem. Mol. Biol.* **2011**, *127*, 27–34. [CrossRef] [PubMed]
5. Quinete, N.; Hauser-Davis, R.A. Drinking water pollutants may affect the immune system: Concerns regarding COVID-19 health effects. *Environ. Sci. Pollut. Res.* **2021**, *28*, 1235–1246. [CrossRef]
6. Available online: http://eurion-cluster.eu (accessed on 8 February 2021).
7. Corrales, J.; Kristofco, L.A.; Steele, W.B.; Yates, B.S.; Breed, C.S.; Williams, E.S.; Brooks, B.W. Global assessment of bisphenol A in the environment: Review and analysis of its occurrence and bioaccumulation. *Dose Response* **2015**, *13*, 1559325815598308. [CrossRef] [PubMed]
8. Zhang, C.; Li, Y.; Wang, C.; Niu, L.; Cai, W. Occurrence of endocrine disrupting compounds in aqueous environment and their bacterial degradation: A review. *Crit. Rev. Environ. Sci. Technol.* **2016**, *46*, 1–59. [CrossRef]
9. Leemans, M.; Couderq, S.; Demeneix, B.; Fini, J.-B. Pesticides with Potential Thyroid Hormone-Disrupting Effects: A Review of Recent Data. *Front. Endocrinol.* **2019**, *10*, 1. [CrossRef]
10. Rezg, R.; El-Fazaa, S.; Gharbi, N.; Mornagui, B. Bisphenol A and human chronic diseases: Current evidences, possible mechanisms, and future perspectives. *Environ. Int.* **2014**, *64*, 83–90. [CrossRef]
11. Ma, Y.; Liu, H.; Wu, J.; Yuan, L.; Wang, Y.; Du, X.; Wang, R.; Marwa, P.W.; Petlulu, P.; Chen, X. The adverse health effects of bisphenol A and related toxicity mechanisms. *Environ. Res.* **2019**, *176*, 108–575. [CrossRef]
12. Shehreen, A.; Md Saidur, R.; Myung-Geol, P. Role of Antioxidants in Alleviating Bisphenol A. *Biomolecules* **2020**, *10*, 1105. [CrossRef]
13. Ragavan, K.V.; Rastogi, N.K.; Thakur, M.S. Review-Sensors and biosensors for analysis of bisphenol-A. *Trends Anal. Chem.* **2013**, *52*, 248–260. [CrossRef]
14. Sarbu, A.; Iordache, T.V.; Florea, A.-M. Trends in the Molecular Imprinting of Small Molecules: Organic and Hybrid Polymers. In *Molecularly Imprinted Polymers (MIPs): Challenges*; Quinn, T., Ed.; NOVA Publishers, Publisher: New York, NY, USA, 2017; pp. 119–174.
15. Kupai, J.; Razali, M.; Buyuktiryaki, S.; Kecili, R.; Szekely, G. Long-term stability and reusability of molecularly imprinted polymers. *Polym. Chem.* **2017**, *8*, 666–673. [CrossRef]
16. Florea, A.M.; Iordache, T.V.; Branger, C.; Ghiurea, M.; Avramescu, S.; Hubca, G.; Sarbu, A. An innovative approach to prepare hypericin molecularly imprinted pearls using a phyto-template. *Talanta* **2016**, *148*, 37–45. [CrossRef] [PubMed]
17. Mba, E.V.; Branger, C.; Bikanga, R.; Florea, A.M.; Istamboulie, G.; Calas-Blanchard, C.; Noguer, T.; Sarbu, A.; Brisset, H. Detection of Bisphenol A in aqueous medium by screen printed carbon electrodes incorporating electrochemical molecularly imprinted polymers. *Biosens. Bioelectron.* **2018**, *112*, 156–161.

18. Florea, A.M.; Iordache, T.V.; Branger, C.; Brisset, H.; Zaharia, A.; Radu, A.L.; Hubca, G.; Sarbu, A. One-step preparation of molecularly imprinted hollow beads for pseudohypericin separation from *Hypericum perforatum* L. Extracts. *Eur. Polym. J.* **2018**, *100*, 48–56. [CrossRef]
19. Lazau, C.; Iordache, T.V.; Florea, A.M.; Orha, C.; Bandas, C.; Radu, A.L.; Sarbu, A.; Rotariu, T. Towards developing an efficient sensitive element for trinitrotoluene detection: TiO2 thin films functionalized with molecularly imprinted copolymer films. *Appl. Surf. Sci.* **2016**, *384*, 449–458. [CrossRef]
20. Yang, Q.; Wu, X.; Peng, H.; Fu, L.; Song, X.; Li, J.; Xiong, H.; Chen, L. Simultaneous phase-inversion and imprinting based sensor for highly sensitive and selective detection of bisphenol A. *Talanta* **2018**, *176*, 595–603. [CrossRef]
21. Stoica, E.-B.G.; Gavrila, A.-M.F.; Iordache, T.-V.; Sarbu, A.; Iovu, H.; Sandu, T.; Brisset, H. Molecularly imprinted membranes obtained via wet phase inversion for ephedrine retention. *U. P. B. Sci. Bull.* **2020**, *82*, 2.
22. Gavrila, A.-M.; Iordache, T.V.; Lazau, C.; Rotariu, T.; Cernica, I.; Stroescu, H.; Stoica, M.; Orha, C.; Bandas, C.E.; Sarbu, A. Biomimetic Sensitive Elements for 2,4,6-Trinitrotoluene Tested on Multi-Layered Sensors. *Coatings* **2020**, *10*, 273. [CrossRef]
23. Boysen, R.I.; Schwarz, L.J.; Nicolau, D.V.; Hearn, M.T. Molecularly imprinted polymer membranes and thin films for the separation and sensing of biomacromolecules. *J. Sep. Sci.* **2017**, *40*, 314–335. [CrossRef] [PubMed]
24. Rechichi, A.; Cristallini, C.; Vitale, U.; Ciardelli, G.; Barbani, N.; Vozzi, G.; Giusti, P. New biomedical devices with selective peptide recognition properties. Part 1: Characterization and cytotoxicity of molecularly imprinted polymers. *J. Cell. Mol. Med.* **2007**, *11*, 1367–1376. [CrossRef]
25. Criscenti, G.; De Maria, C.; Longoni, A.; van Blitterswijk, C.A.; Fernandes, H.A.M.; Vozzi, G.; Moroni, L. Soft-molecular imprinted electrospun scaffolds to mimic specific biological tissues. *Biofabrication* **2018**, *10*, 045005. [CrossRef]
26. Ait-Touchente, Z.; Sakhraoui, H.E.E.Y.; Fourati, N.; Zerrouki, C.; Maouche, N.; Yaakoubi, N.; Touzani, R.; Chehimi, M.M. High Performance Zinc Oxide Nanorod-Doped Ion Imprinted Polypyrrole for the Selective Electrosensing of Mercury II Ions. *Appl. Sci.* **2020**, *10*, 7010. [CrossRef]
27. Zhang, Z.; Li, L.; Wang, H.; Guo, L.; Zhai, Y.; Zhang, J.; Yang, Y.; Wang, H.; Yin, Z.; Yixia, L. Preparation of molecularly imprinted ordered mesoporous silica for rapid and selective separation of trace bisphenol A from water samples. *Appl. Surface Sci.* **2018**, *448*, 380–388. [CrossRef]
28. Gavrila, A.M.; Zaharia, A.; Paruch, L.; Perrin, F.X.; Sarbu, A.; Olaru, A.G.; Paruch, A.M.; Iordache, T.V. Highly efficient materials working in tandem against pathogenic bacteria in wastewaters. *J. Hazard. Mater.* **2020**, *399*, 123026. [CrossRef]
29. Bakas, I.; Hayat, A.; Piletsky, S.; Piletska, E.; Chehimi, M.; Noguer, T.; Rouillon, R. Electrochemical impedimetric sensor based on molecularly imprinted polymers/sol-gel chemistry for methidathion organophosphorous insecticide recognition. *Talanta* **2014**, *130*, 294–298. [CrossRef]
30. Huang, J.; Zhang, X.; Lin, Q.; He, X.; Xing, X.; Huai, H.; Lian, W.; Zhu, H. Electrochemical sensor based on imprinted sol-gel and nanomaterials for sensitive determination of bisphenol A. *Food Control* **2011**, *22*, 786–791. [CrossRef]
31. Yang, J.C.; Park, J. Molecular Imprinting of Bisphenol A on Silica Skeleton and Gold Pinhole Surfaces in 2D Colloidal Inverse Opal through Thermal Graft Copolymerizatio. *Polymers* **2020**, *12*, 1892. [CrossRef]
32. Ardekani, R.; Borhani, S.; Rezaaei, B. Selective molecularly imprinted polymer nanofiber sorbent for the extraction of bisphenol A in a water sample. *Polym. Int.* **2020**, *69*, 780–793. [CrossRef]
33. Kalogiouri, N.P.; Tsalbouris, A.; Kabir, A.; Furton, K.G.; Samanidou, V.F. Synthesis and application of molecularly imprinted polymers using sol–gel matrix imprinting technology for the efficient solid-phase extraction of BPA from water. *Microchem. J.* **2020**, *157*, 104965. [CrossRef]
34. Stoica, E.B.; Gavrila, A.M.; Branger, C.; Brisset, H.; Dyshlyuk, A.V.; Vitrik, O.B.; Iovu, H.; Sarbu, A.; Iordache, T.V. Evaluation of molecularly imprinted thin films for ephedrine recognition. *Mater. Plast.* **2019**, *4*, 865–874. [CrossRef]
35. Zhuang, Y.; Zhou, M.; Gu, J.; Li, X. Spectrophotometric and high performance liquid chromatographic methods for sensitive determination of bisphenol A. *Spectrochim. Acta A Mol. Biomol. Spectrosc.* **2014**, *122*, 153–157. [CrossRef]
36. Florea, A.M.; Sarbu, A.; Donescu, D.; Radu, A.L.; Zaharia, A.; Iordache, T.V. The structure effect upon gallic acid re-binding in molecularly imprinted organosilica. *J. Sol-Gel Sci. Technol.* **2015**, *76*, 529–541. [CrossRef]
37. Gao, P.; Wang, H.; Li, P.; Gao, W.; Zhang, Y.; Chen, J.; Jia, N. In-site synthesis molecular imprinting Nb2O5 –based photoelectrochemical sensor for bisphenol A detection. *Biosens. Bioelectron.* **2018**, *121*, 104–110. [CrossRef] [PubMed]
38. Pei, D.-N.; Zhang, A.-Y.; Pan, X.-Q.; Si, Y.; Yu, H.-Q. Electrochemical Sensing of Bisphenol A on Facet-Tailored TiO2 Single Crystals Engineered by Inorganic-Framework Molecular Imprinting Sites. *Anal. Chem.* **2018**, *90*, 3165–3173. [CrossRef] [PubMed]
39. Liu, R.; Feng, F.; Chen, G.; Liu, Z.; Xu, Z. Barbell-shaped stir barsorptive extraction using dummy template molecularly imprinted polymer coatings for analysis of bisphenol A in water. *Anal. Bioanal. Chem.* **2016**, *408*, 5329–5335. [CrossRef]
40. Anirudhan, T.S.; Athira, V.S.; Chithra Sekhar, V. Electrochemical sensing and nano molar level detection of Bisphenol-A with molecularly imprinted polymer tailored on multiwalled carbon nanotubes. *Polymer* **2018**, *146*, 312–320. [CrossRef]
41. Iordache, T.-V.; Sarbu, A.; Donescu, D.; Nicolae, C.A.; Jerca, F.A.; Dima, S.O. Selecting the nature of imprinted molecular organosilica sieves with gallic acid via thermal analyses. *J. Therm. Anal. Calorim.* **2014**, *118*, 1039–1048. [CrossRef]
42. Shaikh, H.; Sener, G.; Memon, N.; Bhanger, M.I.; Nizamani, S.M.; Üzek, R.; Denizli, A. Molecularly imprinted surface plasmon resonance (SPR) based sensing of bisphenol A for its selective detection in aqueous systems. *Anal. Methods* **2015**, *7*, 4661–4670. [CrossRef]